Journal of Computational Physics 229 (2010) 3691–3705

Contents lists available at ScienceDirect

Journal of Computational Physics

journal homepage: www.elsevier.com/locate/jcp

Stability analysis and time-step limits for a Monte Carlo Compton-scattering method

Jeffery D. Densmore *, James S. Warsa, Robert B. Lowrie

Computational Physics and Methods Group, Los Alamos National Laboratory, P.O. Box 1663, MS D409, Los Alamos, NM 87545, USA

ARTICLE INFO

Article history:
Received 19 October 2009
Received in revised form 14 January 2010
Accepted 18 January 2010
Available online 25 January 2010

Keywords:
Radiative transfer
Compton scattering
Monte Carlo
Stability analysis
Time-step limit

ABSTRACT

A Monte Carlo method for simulating Compton scattering in high energy density applications has been presented that models the photon–electron collision kinematics exactly [E. Canfield, W.M. Howard, E.P. Liang, Inverse Comptonization by one-dimensional relativistic electrons, Astrophys. J. 323 (1987) 565]. However, implementing this technique typically requires an explicit evaluation of the material temperature, which can lead to unstable and oscillatory solutions. In this paper, we perform a stability analysis of this Monte Carlo method and develop two time-step limits that avoid undesirable behavior. The first time-step limit prevents instabilities, while the second, more restrictive time-step limit avoids both instabilities and nonphysical oscillations. With a set of numerical examples, we demonstrate the efficacy of these time-step limits.

1. Introduction

Compton scattering is an important aspect of radiative transfer in high energy density applications [1]. In this process, a photon collides with a free electron, altering the frequency and direction of the photon. The change in frequency of a scattered photon corresponds to an energy exchange between the photon and electron, which in turn affects the material energy and temperature. Canfield et al. have presented a Monte Carlo method for simulating Compton scattering that models the photon–electron collision kinematics exactly [2]. However, because this technique involves sampling electron velocities from a distribution that is a function of the material temperature, implementing it in problems where the material temperature can vary in time typically requires approximating the temperature dependence of this distribution explicitly. This explicit evaluation can lead to unstable and oscillatory solutions.

In this paper, we perform a stability analysis of this Monte Carlo Compton-scattering method and present time-step limits that avoid undesirable behavior [3]. To facilitate this work, we consider the Monte Carlo simulation of a spatially independent, purely scattering radiative-transfer problem in which Compton scattering is treated with this Monte Carlo technique. Examining a simplified problem is justified because it isolates the effects of Compton scattering and existing Monte Carlo methods can robustly model other physics [4,5] (such as absorption, emission, sources, and photon streaming). Our analysis begins by simplifying the equations that are solved via Monte Carlo within each time step using the Fokker–Planck approximation [6–9]. Next, we linearize these approximate equations about an equilibrium solution such that the resulting linearized equations describe perturbations about this equilibrium. We then solve these linearized equations over a time step and determine the corresponding eigenvalues, quantities that can predict the behavior of solutions generated by a Monte Carlo simulation as a function of time-step size and other physical parameters. With these results, we develop two time-step

* Corresponding author. Tel.: +1 505 665 9198.
E-mail addresses: jdd@lanl.gov (J.D. Densmore), warsa@lanl.gov (J.S. Warsa), lowrie@lanl.gov (R.B. Lowrie).

0021-9991/$ - see front matter © 2010 Elsevier Inc. All rights reserved.
doi:10.1016/j.jcp.2010.01.022

limits. The first time-step limit prevents instabilities, while the second, more restrictive time-step limit avoids both instabilities *and* nonphysical oscillations.

The approach described above is similar to our recent investigation of time discretizations for the Compton-scattering Fokker–Planck equation [10]. In fact, our hope was to apply the time-step limits corresponding to a semi-implicit discretization, i.e., a combination of backward-Euler differencing and explicitly approximated temperature-dependent quantities, directly to Monte Carlo simulations. Unfortunately, although sufficient for this semi-implicit discretization, we found that these time-step limits were too large when used with Monte Carlo in the sense that they allowed undesirable behavior; a semi-implicit discretization of the Fokker–Planck equation is apparently somehow "more stable" than a Monte Carlo simulation in which the only approximation is an explicit evaluation of the material temperature. Thus, we were led to develop the time-step limits in this paper.

We begin the remainder of this paper by presenting our simplified radiative-transfer problem and discussing its solution by Monte Carlo. We then perform our stability analysis, which we follow by developing our time-step limits. Next, we demonstrate the effectiveness of these time-step limits using a set of numerical examples. We conclude with a brief discussion.

2. Radiative transfer, Compton scattering, and Monte Carlo

The specific radiative-transfer problem we examine is described by [1]

$$\frac{1}{c}\frac{\partial I}{\partial t}+\sigma_s I=\iint\frac{\nu}{\nu'}\sigma_s(\nu'\to\nu,\boldsymbol{\Omega}'\cdot\boldsymbol{\Omega},T)I(\nu',\boldsymbol{\Omega}',t)d\nu'\,d\boldsymbol{\Omega}', \tag{1}$$

and

$$\frac{dU}{dt}=\iiiint\left(1-\frac{\nu}{\nu'}\right)\sigma_s(\nu'\to\nu,\boldsymbol{\Omega}'\cdot\boldsymbol{\Omega},T)I(\nu',\boldsymbol{\Omega}',t)d\nu'\,d\boldsymbol{\Omega}'\,d\nu\,d\boldsymbol{\Omega}. \tag{2}$$

Here, ν is the photon frequency, $\boldsymbol{\Omega}$ is the photon direction, t is the temporal variable, $I(\nu,\boldsymbol{\Omega},t)$ is the radiation intensity, $T(t)$ is the material temperature, $\sigma_s(\nu,T)$ is the total scattering opacity, $\sigma_s(\nu'\to\nu,\boldsymbol{\Omega}'\cdot\boldsymbol{\Omega},T)$ is the differential scattering opacity, and c is the speed of light. In addition, the material energy density $U(T)$ is related to the material temperature through

$$\frac{dU}{dT}=C_v, \tag{3}$$

where $C_v(T)$ is the heat capacity. Note that we have neglected induced scattering in Eqs. (1) and (2), a physical effect that would make these expressions nonlinear functions of the radiation intensity.

The differential scattering opacity, which models Compton scattering, has a complicated dependence on the material temperature [1],

$$\sigma_s(\nu'\to\nu,\boldsymbol{\Omega}'\cdot\boldsymbol{\Omega},T)=N_e\int\sqrt{1-v^2/c^2}\,\frac{1-\boldsymbol{\Omega}'\cdot\mathbf{v}/c}{1-\boldsymbol{\Omega}\cdot\mathbf{v}/c}\,\mu_{\mathrm{KN}}(\nu_0'\to\nu_0,\boldsymbol{\Omega}_0'\cdot\boldsymbol{\Omega}_0)f(\mathbf{v},T)d\mathbf{v}. \tag{4}$$

In this expression, N_e is the electron density, $\mathbf{v}$ is the electron velocity, $\mu_{\mathrm{KN}}(\nu_0'\to\nu_0,\boldsymbol{\Omega}_0'\cdot\boldsymbol{\Omega}_0)$ is the Klein–Nishina differential scattering cross section, and $f(\mathbf{v},T)$ is the electron velocity distribution. The electron velocity distribution is a relativistic Maxwellian of the form

$$f(\mathbf{v},T)=\frac{1}{4\pi c^3}\frac{mc^2}{kT}\frac{e^{-mc^2/\left(kT\sqrt{1-v^2/c^2}\right)}}{\left(1-v^2/c^2\right)^{5/2}K_2(mc^2/kT)}, \tag{5}$$

where k is Boltzmann's constant, mc^2 is the electron rest mass in energy units, and K_2 is the modified Bessel function of the second kind of order two [11]. Also, the Klein–Nishina differential scattering cross section, which is valid in the electron rest frame, is

$$\mu_{\mathrm{KN}}(\nu_0'\to\nu_0,\boldsymbol{\Omega}_0'\cdot\boldsymbol{\Omega}_0)=\frac{3}{16\pi}\mu_{\mathrm{Th}}\frac{mc^2}{h(\nu_0')^2}\left[1+(\boldsymbol{\Omega}_0'\cdot\boldsymbol{\Omega}_0)^2+\frac{h\nu_0'}{mc^2}\frac{h\nu_0}{mc^2}(1-\boldsymbol{\Omega}_0'\cdot\boldsymbol{\Omega}_0)^2\right]\delta\left(\boldsymbol{\Omega}_0'\cdot\boldsymbol{\Omega}_0-1+\frac{mc^2}{h\nu_0}-\frac{mc^2}{h\nu_0'}\right). \tag{6}$$

Here, μ_{Th} is the Thomson cross section, h is Planck's constant, and the subscript 0 denotes photon properties in the electron rest frame. For a given value of the electron velocity, these rest-frame properties can be related to their laboratory-frame counterparts with a Lorentz transformation [1,12]. The total scattering opacity is simply the differential scattering opacity integrated over all outgoing frequencies and directions,

$$\sigma_s(\nu,T)=\iint\sigma_s(\nu\to\nu',\boldsymbol{\Omega}\cdot\boldsymbol{\Omega}',T)d\nu'\,d\boldsymbol{\Omega}'. \tag{7}$$

Two quantities of interest derived from the radiation intensity are the spectral radiation energy density,

$$E(\nu,t)=\frac{1}{c}\int I(\nu,\boldsymbol{\Omega},t)d\boldsymbol{\Omega}, \tag{8}$$

and the total radiation energy density,

$$\mathcal{E}(t) = \frac{1}{c}\iint I(v,\mathbf{\Omega},t)d\mathbf{\Omega}\,dv = \int E(v,t)dv. \tag{9}$$

Because we have not included absorption, emission, or induced scattering in Eqs. (1) and (2), the equilibrium spectral radiation energy density in this case is given by a Wien distribution:

$$W(v,T) = \frac{hN_p}{2}\left(\frac{hv}{kT}\right)^3 e^{-hv/kT}. \tag{10}$$

In this expression, N_p is the photon density. Substituting Eq. (10) into Eq. (9) yields the total radiation energy density corresponding to a Wien distribution,

$$\mathcal{E}(T) = 3kTN_p. \tag{11}$$

Furthermore, we can define a radiation heat capacity in a manner similar to Eq. (3) by differentiating Eq. (11) with respect to temperature,

$$C_r = \frac{d\mathcal{E}}{dT} = 3kN_p. \tag{12}$$

To solve Eqs. (1) and (2) using Monte Carlo, we first prescribe a temporal grid $0 = t_0 < t_1 < t_2 < \cdots$. Then, within each time step $t_n < t \leqslant t_{n+1}$, we explicitly approximate the temperature dependence of the total and differential scattering opacities and write Eq. (1) as

$$\frac{1}{c}\frac{\partial I}{\partial t} + \sigma_{s,n}I = \iint \frac{v}{v'}\sigma_s(v' \to v, \mathbf{\Omega}'\cdot\mathbf{\Omega}, T_n)I(v',\mathbf{\Omega}',t)dv'\,d\mathbf{\Omega}', \tag{13}$$

whereas further integrating Eq. (2) over the time step results in

$$U_{n+1} - U_n = \int_{t_n}^{t_{n+1}}\iiiint \left(1 - \frac{v}{v'}\right)\sigma_s(v' \to v, \mathbf{\Omega}'\cdot\mathbf{\Omega}, T_n)I(v',\mathbf{\Omega}',t)dv'\,d\mathbf{\Omega}'\,dv\,d\mathbf{\Omega}\,dt. \tag{14}$$

The subscript n in Eqs. (13) and (14) denotes quantities evaluated at time t_n. For each time step, we can determine the radiation intensity from Eq. (13) with standard Monte Carlo methods. When a particle scatters, its new frequency and direction are calculated as follows [2]:

1. sample a tentative electron velocity;
2. Lorentz transform the incident frequency and direction to the electron rest frame;
3. accept the electron velocity based on the value of the Klein–Nishina total scattering cross section [i.e., Eq. (6) integrated over all outgoing rest-frame frequencies and directions], otherwise reject the electron velocity and return to the first step;
4. determine the outgoing frequency and direction in the electron rest frame according to the Klein–Nishina differential scattering cross section;
5. Lorentz transform the outgoing frequency and direction back to the laboratory frame.

A complete description of this procedure is given in Ref. [2]. We note, however, that the fourth step above can be performed using existing techniques [13,14], while in the first step the electron velocity is sampled from the temperature-dependent distribution in Eq. (5), the same distribution that contains the temperature dependence of the total and differential scattering opacities. Because this distribution must be fully specified at the start of each time step before the Monte Carlo simulation begins, we employ the beginning-of-time-step value of the material temperature to process scattering events; it is for this reason that we have evaluated the total and differential scattering opacities in Eqs. (13) and (14) explicitly. At the end of each time step, we can update the material temperature through Eqs. (3) and (14).

3. Stability analysis

We begin our stability analysis by simplifying Eqs. (13) and (14) using the Fokker–Planck approximation [6–9],

$$\frac{1}{\sigma_{\mathrm{Th}}c}\frac{\partial E}{\partial t} = v\frac{\partial}{\partial v}\left[v\frac{kT_n}{mc^2}\frac{\partial E}{\partial v} + \left(\frac{hv}{mc^2} - 3\frac{kT_n}{mc^2}\right)E\right], \tag{15}$$

and

$$U_{n+1} - U_n = -\sigma_{\mathrm{Th}}c\int_{t_n}^{t_{n+1}}\int v\frac{\partial}{\partial v}\left[v\frac{kT_n}{mc^2}\frac{\partial E}{\partial v} + \left(\frac{hv}{mc^2} - 3\frac{kT_n}{mc^2}\right)E\right]dv\,dt = -\int (E_{n+1} - E_n)dv. \tag{16}$$

The second equality in Eq. (16) follows from Eq. (15). In these two expression, σ_{Th} is the Thomson opacity,

$$\sigma_{\mathrm{Th}} = N_e \mu_{\mathrm{Th}}. \tag{17}$$

The Fokker–Planck approximation is valid when the photon frequency and material temperature are small with respect to the electron rest mass, i.e.,

$$\frac{h\nu}{mc^2} \ll 1 \quad \text{and} \quad \frac{kT_n}{mc^2} \ll 1. \tag{18}$$

Although these conditions are not always satisfied in practice, our ultimate goal in employing this approximation is to generate time-step limits, not actual solutions.

Next, we linearize Eqs. (15) and (16) by first expressing the material temperature and spectral radiation energy density as

$$T_n = T + \delta T_n, \tag{19}$$

and

$$E(\nu, t) = W(\nu, T) + \delta E(\nu, t). \tag{20}$$

Here, δT_n and δE are (ideally small) perturbations in the material temperature and spectral radiation energy density, respectively, about their equilibrium values, and T is now the equilibrium material temperature. When we substitute Eqs. (19) and (20) into Eq. (15), ignore terms of order $O(\delta T_n \delta E)$, and make use of Eq. (10), we have

$$\frac{1}{\sigma_{\mathrm{Th}} c}\frac{\partial}{\partial t}\delta E = \nu \frac{\partial}{\partial \nu}\left[\nu \frac{kT}{mc^2}\frac{\partial}{\partial \nu}\delta E + \left(\frac{h\nu}{mc^2} - 3\frac{kT}{mc^2}\right)\delta E\right] + \frac{hN_p}{2}\frac{k\delta T_n}{mc^2}\left[\left(\frac{h\nu}{kT}\right)^5 - 4\left(\frac{h\nu}{kT}\right)^4\right] e^{-h\nu/kT}, \tag{21}$$

which is the linearized version of Eq. (15). In fact, Eq. (21) is of the same form as Eq. (15), except there is now a source term on the right side that is proportional to the material-temperature perturbation. Also, evaluating Eq. (16) with Eqs. (19) and (20) yields

$$U(T + \delta T_{n+1}) + \int \delta E_{n+1}\, d\nu = U(T + \delta T_n) + \int \delta E_n\, d\nu. \tag{22}$$

If we expand $U(T + \delta T_n)$ in a Taylor series about T, apply Eq. (3), and ignore terms of order $O(\delta T_n^2)$, we can write

$$\begin{aligned} U(T + \delta T_n) &= U(T) + \delta T_n \frac{dU}{dT} + O(\delta T_n^2) \\ &\approx U(T) + C_\nu(T)\delta T_n. \end{aligned} \tag{23}$$

Combining Eqs. (22) and (23) gives the linearized version of Eq. (16),

$$C_\nu(T)\delta T_{n+1} + \int \delta E_{n+1}\, d\nu = C_\nu(T)\delta T_n + \int \delta E_n\, d\nu. \tag{24}$$

For more details regarding this linearization process, see Ref. [10].

We can simplify Eqs. (21) and (24) by defining the following dimensionless transformations:

$$\frac{h\nu}{kT} \to x; \tag{25}$$

$$\frac{kT}{mc^2}\sigma_{\mathrm{Th}} ct \to t; \tag{26}$$

$$\frac{\delta E(\nu, t)}{hN_p} \to \delta E(x, t); \tag{27}$$

$$\frac{\delta T_n}{T} \to \delta T_n; \tag{28}$$

$$\frac{C_\nu(T)}{kN_p} \to C_\nu. \tag{29}$$

Note that x represents a nondimensional photon frequency. Using Eqs. (25)–(29) allows us to express Eqs. (21) and (24) as

$$\frac{\partial}{\partial t}\delta E = M\delta E + \delta T_n F, \tag{30}$$

and

$$C_\nu \delta T_{n+1} + \int_0^\infty \delta E_{n+1}\, dx = C_\nu \delta T_n + \int_0^\infty \delta E_n\, dx, \tag{31}$$

where it is understood that all quantities are dimensionless. In Eq. (30), M is the nondimensional Fokker–Planck operator,

$$M\delta E = x^2 \frac{\partial^2}{\partial x^2}\delta E + x(x-2)\frac{\partial}{\partial x}\delta E + x\delta E, \tag{32}$$

and

$$F(x) = \frac{1}{2}(x^5 - 4x^4)e^{-x}. \tag{33}$$

We continue by solving Eqs. (30) and (31) over a time step. This step was not necessary in our previous stability analysis of time discretizations for the Compton-scattering Fokker–Planck equation because only quantities evaluated at the beginning and end of a time step were involved in this case [10]. To represent the frequency dependence of δE, we employ an expansion based on the eigenfunctions of M. The eigenvalue problem of interest is then

$$My_\lambda + \lambda y_\lambda = 0. \tag{34}$$

Here, $y_\lambda(x)$ is an eigenfunction of M and λ is the corresponding eigenvalue. Kompaneets [6] and Pomraning [15] have shown that the solution to Eq. (34) consists of two discrete eigenfunction–eigenvalue pairs,

$$y_0(x) = \frac{1}{\sqrt{2}}x^3e^{-x}, \quad \lambda = 0, \tag{35}$$

and

$$y_2(x) = \frac{1}{\sqrt{2}}(x^3 - 2x^2)e^{-x}, \quad \lambda = 2, \tag{36}$$

and a continuum of eigenfunction–eigenvalue pairs,

$$y_\lambda(x) = \sqrt{\frac{\sinh[\pi a(\lambda)]}{\pi\lambda(\lambda-2)}}x^{3/2+ia(\lambda)}e^{-x}\Psi[-3/2 + ia(\lambda), 1 + 2ia(\lambda); x], \quad \lambda \geqslant 9/4. \tag{37}$$

In Eq. (37), Ψ is the confluent hypergeometric function of the second kind [16] and a is given by

$$a(\lambda) = \sqrt{\lambda - \frac{9}{4}}. \tag{38}$$

These eigenfunctions are orthogonal with respect to the weighting function [15]

$$w(x) = \frac{e^x}{x^4}. \tag{39}$$

Thus, an arbitrary function $f(x)$ may be expanded as

$$f = c_0y_0 + c_2y_2 + \int_{9/4}^{\infty} c_\lambda y_\lambda\, d\lambda, \tag{40}$$

where the coefficients in this expansion are defined by

$$c_0 = \int_0^\infty f(x)y_0(x)w(x)dx, \tag{41}$$

$$c_2 = \int_0^\infty f(x)y_2(x)w(x)dx, \tag{42}$$

and

$$c_\lambda = \int_0^\infty f(x)y_\lambda(x)w(x)dx. \tag{43}$$

Therefore, we express δE using

$$\delta E = \alpha_0y_0 + \alpha_2y_2 + \int_{9/4}^{\infty} \alpha_\lambda y_\lambda\, d\lambda. \tag{44}$$

Here, $\alpha_0(t)$, $\alpha_2(t)$, and $\alpha_\lambda(t)$ are time-dependent expansion coefficients that are yet to be determined. A similar expansion of Eq. (33) is [10]

$$F = \beta_0y_0 + \beta_2y_2 + \int_{9/4}^{\infty} \beta_\lambda y_\lambda\, d\lambda, \tag{45}$$

with

$$\beta_0 = 0, \tag{46}$$

$$\beta_2 = \sqrt{2}, \tag{47}$$

and

$$\beta_\lambda = \frac{\pi}{2}\frac{\lambda^2(\lambda-2)}{\cosh[\pi a(\lambda)]}\sqrt{\frac{\sinh[\pi a(\lambda)]}{\pi\lambda(\lambda-2)}}. \tag{48}$$

Substituting Eq. (44) into Eq. (30) and applying Eqs. (34), (45), (46), (47), and the orthogonality of Eqs. (35)–(37) shows that α_0, α_2, and α_λ must satisfy

$$\frac{d}{dt}\alpha_0 = 0, \tag{49}$$

$$\frac{d}{dt}\alpha_2 = -2\alpha_2 + \sqrt{2}\delta T_n, \tag{50}$$

and

$$\frac{d}{dt}\alpha_\lambda = -\lambda\alpha_\lambda + \beta_\lambda \delta T_n. \tag{51}$$

When we solve Eqs. (49)–(51), we see that the end-of-time-step values of these expansion coefficients are related to their beginning-of-time-step counterparts by

$$\alpha_{0,n+1} = \alpha_{0,n}, \tag{52}$$

$$\alpha_{2,n+1} = \alpha_{2,n}e^{-2\Delta t} + \frac{1}{\sqrt{2}}(1-e^{-2\Delta t})\delta T_n, \tag{53}$$

and

$$\alpha_{\lambda,n+1} = \alpha_{\lambda,n}e^{-\lambda\Delta t} + \frac{\beta_\lambda}{\lambda}(1-e^{-\lambda\Delta t})\delta T_n. \tag{54}$$

In Eqs. (53) and (54), $\Delta t = t_{n+1} - t_n$ is the time-step size, a quantity that for simplicity we assume is constant. Also, evaluating Eq. (31) with Eq. (44) yields

$$C_v(\delta T_{n+1} - \delta T_n) + 3\sqrt{2}(\alpha_{0,n+1} - \alpha_{0,n}) + \sqrt{2}(\alpha_{2,n+1} - \alpha_{2,n}) + \int_{9/4}^{\infty}\frac{2}{\lambda}\beta_\lambda(\alpha_{\lambda,n+1} - \alpha_{\lambda,n})d\lambda = 0, \tag{55}$$

where we have made use of

$$\int_0^\infty y_0\,dx = 3\sqrt{2}, \tag{56}$$

$$\int_0^\infty y_2\,dx = \sqrt{2}, \tag{57}$$

and [10]

$$\int_0^\infty y_\lambda\,dx = \frac{\pi\lambda(\lambda-2)}{\cosh[\pi a(\lambda)]}\sqrt{\frac{\sinh[\pi a(\lambda)]}{\pi\lambda(\lambda-2)}} = \frac{2}{\lambda}\beta_\lambda. \tag{58}$$

Eqs. (52)–(55) represent a complete solution of Eqs. (30) and (31) over a time step, that is, they determine δT_{n+1} and the expansion coefficients of δE_{n+1} in terms of δT_n and the expansion coefficients of δE_n.

We now look for solutions to Eqs. (52)–(55) of the form

$$\alpha_{0,n} = \omega^n\alpha_0, \tag{59}$$

$$\alpha_{2,n} = \omega^n\alpha_2, \tag{60}$$

$$\alpha_{\lambda,n} = \omega^n\alpha_\lambda, \tag{61}$$

and

$$\delta T_n = \omega^n\delta T. \tag{62}$$

Here, α_0, α_2, α_λ, and δT are components of an eigenfunction of Eqs. (52)–(55), while ω is the corresponding eigenvalue or *amplification factor*. Amplification factors provide insight into the behavior of solutions to Eqs. (52)–(55), and consequently Eqs. (30) and (31), as a function of time-step size and other physical parameters. For example, if $|\omega| > 1$, then from Eqs. (59)–(62) the magnitude of the solution can grow without bound, in which case the solution is considered unstable. In addition, if $\omega < 0$, then Eqs. (59)–(62) show that the solution can nonphysically oscillate. (We will prove that there are no complex amplification factors in Appendix A). This approach is somewhat similar to von Neumann analysis, the standard method for investigating stability properties of time-discretization schemes [17]. Furthermore, if the Fokker–Planck approximation is accurate such that the conditions in Eq. (18) are satisfied, and our linearization process is valid such that the perturbations

in Eqs. (19) and (20) are sufficiently small, then the amplification factors for Eqs. (52)–(55) should also predict the behavior of Monte Carlo-generated solutions to Eqs. (13) and (14).

When we substitute Eqs. (59)–(62) into Eqs. (52)–(55), we have

$$(\omega - 1)\alpha_0 = 0, \tag{63}$$

$$(\omega - e^{-2\Delta t})\alpha_2 = \frac{1}{\sqrt{2}}(1 - e^{-2\Delta t})\delta T, \tag{64}$$

$$(\omega - e^{-\lambda\Delta t})\alpha_\lambda = \frac{\beta_\lambda}{\lambda}(1 - e^{-\lambda\Delta t})\delta T, \tag{65}$$

and

$$(\omega - 1)\left(C_v\delta T + 3\sqrt{2}\alpha_0 + \sqrt{2}\alpha_2 + \int_{9/4}^{\infty}\frac{2}{\lambda}\beta_\lambda\alpha_\lambda\, d\lambda\right) = 0. \tag{66}$$

We can now use Eqs. (63)–(66) to determine valid amplification factors. However, care must be taken when solving Eqs. (63)–(65) for α_0, α_2, and α_λ as the terms in parentheses on the left sides of these expressions are possibly zero, and thus a straightforward solution may lead to singular quantities. Specifically, we see from Eqs. (63) and (64) that there are discrete singularities at $\omega = 1$ and $\omega = \omega_1$, where

$$\omega_1 = e^{-2\Delta t}. \tag{67}$$

In addition, because λ varies from 9/4 to infinity, Eq. (65) shows that there is a continuum of singularities for $0 < \omega \leqslant \omega_2$, where

$$\omega_2 = e^{-9/4\Delta t}. \tag{68}$$

Fortunately, these singularities represent values of ω that are neither negative nor greater than unity in magnitude and thus cannot cause instabilities or nonphysical oscillations. If we avoid these singularities and disregard any corresponding amplification factors, we can directly solve Eqs. (63)–(65) to write

$$\alpha_0 = 0, \tag{69}$$

$$\alpha_2 = \frac{1}{\sqrt{2}}\frac{1 - e^{-2\Delta t}}{\omega - e^{-2\Delta t}}\delta T, \tag{70}$$

and

$$\alpha_\lambda = \frac{\beta_\lambda}{\lambda}\frac{1 - e^{-\lambda\Delta t}}{\omega - e^{-\lambda\Delta t}}\delta T. \tag{71}$$

Also, satisfying Eq. (66) in this case requires

$$C_v\delta T + 3\sqrt{2}\alpha_0 + \sqrt{2}\alpha_2 + \int_{9/4}^{\infty}\frac{2}{\lambda}\beta_\lambda\alpha_\lambda = 0. \tag{72}$$

Then, evaluating Eq. (72) with Eqs. (69)–(71) and making use of Eq. (48) allows us to define a characteristic equation for the remaining amplification factors as

$$H(\omega) = 0, \tag{73}$$

where

$$H(\omega) = C_v + \frac{1 - e^{-2\Delta t}}{\omega - e^{-2\Delta t}} + \frac{\pi}{2}\int_{9/4}^{\infty}\lambda(\lambda - 2)\frac{1 - e^{-\lambda\Delta t}}{\omega - e^{-\lambda\Delta t}}\frac{\tanh[\pi a(\lambda)]}{\cosh[\pi a(\lambda)]}\, d\lambda. \tag{74}$$

Valid amplification factors are roots of the characteristic equation such that they satisfy Eq. (73).

An inspection of Eq. (74) reveals that H has the following properties:

$$\lim_{\omega\to\pm\infty} H(\omega) = C_v > 0; \tag{75}$$

$$\frac{dH}{d\omega} = -\frac{1 - e^{-2\Delta t}}{(\omega - e^{-2\Delta t})^2} - \frac{\pi}{2}\int_{9/4}^{\infty}\lambda(\lambda - 2)\frac{1 - e^{-\lambda\Delta t}}{(\omega - e^{-\lambda\Delta t})^2}\frac{\tanh[\pi a(\lambda)]}{\cosh[\pi a(\lambda)]}\, d\lambda < 0. \tag{76}$$

In addition, we see that H diverges to negative infinity as ω approaches ω_1 from the left and diverges to positive infinity as ω approaches ω_1 from the right. With these characteristics of H, we can predict the locations of solutions to Eq. (73):

- $\omega \leqslant 0$: In this region, H monotonically decreases from its asymptotic value of C_v to $H(0)$. Thus, there is a single root if $H(0) \leqslant 0$. Otherwise, there are no roots.
- $\omega_2 < \omega < \omega_1$: Here, H monotonically decreases to negative infinity. Thus, there is a single root if H is positive near ω_2. Otherwise, there are no roots.
- $\omega_1 < \omega$: In this region, H monotonically decreases from positive infinity to its asymptotic value of C_v. Thus, there are no roots.

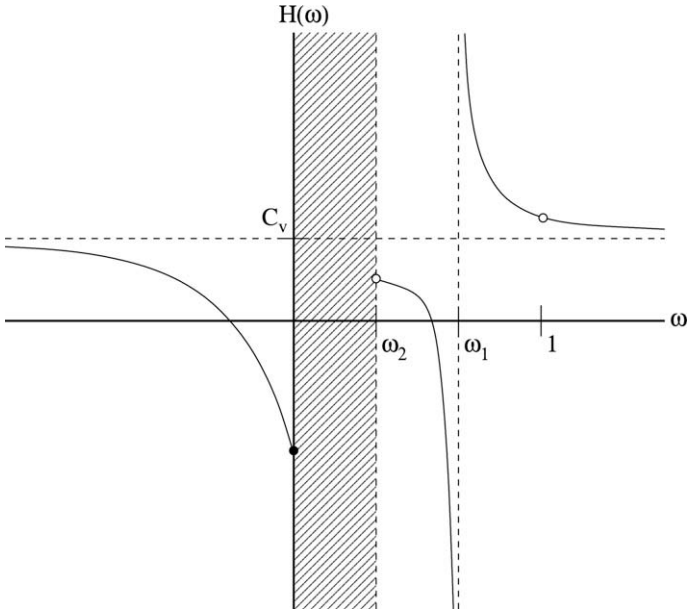

Fig. 1. An example of $H(\omega)$.

Eqs. (67) and (68) show that if there is a root satisfying $\omega_2 < \omega < \omega_1$, this root is positive and less than unity and cannot produce undesirable behavior. Therefore, only the existence and location of the nonpositive root can predict the occurrence of unstable and oscillatory solutions.

In Fig. 1, we plot an example of H for specific values of C_v and Δt. Note that this function is not defined in the shaded region $(0 < \omega < \omega_2)$ or at $\omega = 1$. Although we have depicted a nonpositive root and a root satisfying $\omega_2 < \omega < \omega_1$, in reality these roots may or may not exist depending on the actual values of C_v and Δt.

4. Time-step limits

In the previous section, we found that we only need to consider the nonpositive root of Eq. (73) in order to predict whether solutions of Eqs. (30) and (31), and ideally those of Eqs. (13) and (14) generated by a Monte Carlo simulation, will be unstable or exhibit nonphysical oscillations. We now make use of this fact to develop two time-step limits that avoid undesirable behavior.

We first present a time-step limit that prevents amplification factors less than negative one and the accompanying instabilities. As discussed above, H is a monotonically decreasing function of ω for $\omega \leqslant 0$. Thus, we can ensure that there are no roots of Eq. (73) less than negative one by requiring H be non-negative at this value,

$$H(-1) \geqslant 0. \tag{77}$$

Combining Eqs. (74) and (77) reveals that the time-step size must satisfy

$$C_v - \frac{1-e^{-2\Delta t}}{1+e^{-2\Delta t}} - \frac{\pi}{2}\int_{9/4}^{\infty} \lambda(\lambda-2)\frac{1-e^{-\lambda\Delta t}}{1+e^{-\lambda\Delta t}}\frac{\tanh[\pi a(\lambda)]}{\cosh[\pi a(\lambda)]}\,d\lambda \geqslant 0. \tag{78}$$

The left side of this expression is a monotonically decreasing function of Δt,

$$\begin{aligned}\frac{d}{d\Delta t}&\left\{C_v - \frac{1-e^{-2\Delta t}}{1+e^{-2\Delta t}} - \frac{\pi}{2}\int_{9/4}^{\infty} \lambda(\lambda-2)\frac{1-e^{-\lambda\Delta t}}{1+e^{-\lambda\Delta t}}\frac{\tanh[\pi a(\lambda)]}{\cosh[\pi a(\lambda)]}\,d\lambda\right\}\\ &= -4\frac{e^{-2\Delta t}}{(1+e^{-2\Delta t})^2} - \pi\int_{9/4}^{\infty}\lambda^2(\lambda-2)\frac{e^{-\lambda\Delta t}}{(1+e^{-\lambda\Delta t})^2}\frac{\tanh[\pi a(\lambda)]}{\cosh[\pi a(\lambda)]}\,d\lambda < 0,\end{aligned} \tag{79}$$

and has a minimum value of

$$\lim_{\Delta t\to\infty}\left\{C_v - \frac{1-e^{-2\Delta t}}{1+e^{-2\Delta t}} - \frac{\pi}{2}\int_{9/4}^{\infty} \lambda(\lambda-2)\frac{1-e^{-\lambda\Delta t}}{1+e^{-\lambda\Delta t}}\frac{\tanh[\pi a(\lambda)]}{\cosh[\pi a(\lambda)]}\,d\lambda\right\} = C_v - 1 - \frac{\pi}{2}\int_{9/4}^{\infty}\lambda(\lambda-2)\frac{\tanh[\pi a(\lambda)]}{\cosh[\pi a(\lambda)]}\,d\lambda. \tag{80}$$

We can evaluate the right side of Eq. (80) with Eq. (118),

$$\int_{9/4}^{\infty} \lambda(\lambda-2)\frac{\tanh[\pi a(\lambda)]}{\cosh[\pi a(\lambda)]} = \frac{4}{\pi}. \tag{81}$$

Eq. (80) then becomes

$$\lim_{\Delta t\to\infty}\left\{C_v - \frac{1-e^{-2\Delta t}}{1+e^{-2\Delta t}} - \frac{\pi}{2}\int_{9/4}^{\infty}\lambda(\lambda-2)\frac{1-e^{-\lambda\Delta t}}{1+e^{-\lambda\Delta t}}\frac{\tanh[\pi a(\lambda)]}{\cosh[\pi a(\lambda)]}\,d\lambda\right\} = C_v - 3. \tag{82}$$

Therefore, Eq. (78) is always met regardless of time-step size if

$$C_v \geqslant 3. \tag{83}$$

Casting Eq. (83) into dimensional units via Eq. (29) yields

$$C_v(T) \geqslant 3kN_p, \tag{84}$$

or, after applying Eq. (12),

$$C_v(T) \geqslant C_r. \tag{85}$$

Eq. (85) has the interpretation that when the material heat capacity is larger than the radiation heat capacity, we can expect the material temperature to vary more slowly in time than the radiation intensity, and it is appropriate to explicitly approximate the temperature dependence of the total and differential scattering opacities in Eqs. (13) and (14).

If Eq. (85) is not satisfied, we are compelled to solve Eq. (78) numerically for the corresponding time-step limit. This process is most likely impractical. As an alternative, we expand Eq. (78) in a Taylor series about $\Delta t = 0$,

$$C_v - \left\{1 + \frac{\pi}{4}\int_{9/4}^{\infty}\lambda^2(\lambda-2)\frac{\tanh[\pi a(\lambda)]}{\cosh[\pi a(\lambda)]}\,d\lambda\right\}\Delta t + O(\Delta t^3) \geqslant 0, \tag{86}$$

where the $O(\Delta t^2)$ term is identically zero. For sufficiently small values of Δt, Eq. (86) should be an accurate approximation of Eq. (78). Using Eq. (119),

$$\int_{9/4}^{\infty}\lambda^2(\lambda-2)\frac{\tanh[\pi a(\lambda)]}{\cosh[\pi a(\lambda)]}\,d\lambda = \frac{20}{\pi}, \tag{87}$$

and ignoring the $O(\Delta t^3)$ term allows us to write Eq. (86) as

$$C_v - 6\Delta t \geqslant 0. \tag{88}$$

When we solve this expression for Δt and transform the results into dimensional units through Eqs. (26) and (29), we see that an approximate time-step limit is

$$\Delta t \leqslant \frac{1}{6}\frac{1}{\sigma_{\mathrm{Th}}c}\frac{mc^2}{kT}\frac{C_v(T)}{kN_p}. \tag{89}$$

A more restrictive condition that avoids both instabilities and nonphysical oscillations is to instead prevent negative amplification factors altogether. Analogous to Eq. (77), we require in this case that H is non-negative at zero,

$$H(0) \geqslant 0. \tag{90}$$

Substituting Eq. (74) into Eq. (90) shows that the time-step size must now satisfy

$$C_v + 1 - e^{2\Delta t} + \frac{\pi}{2}\lim_{\omega\to 0^-}\int_{9/4}^{\infty}\lambda(\lambda-2)\frac{1-e^{-\lambda\Delta t}}{\omega - e^{-\lambda\Delta t}}\frac{\tanh[\pi a(\lambda)]}{\cosh[\pi a(\lambda)]}\,d\lambda \geqslant 0. \tag{91}$$

To determine the actual value of the time-step limit from Eq. (91), we again need a numerical calculation. We can develop an approximate time-step limit by applying a Taylor-series expansion to Eq. (91) in a manner similar to Eq. (86),

$$C_v - \left\{2 + \frac{\pi}{2}\int_{9/4}^{\infty}\lambda^2(\lambda-2)\frac{\tanh[\pi a(\lambda)]}{\cosh[\pi a(\lambda)]}\,d\lambda\right\}\Delta t - \left\{2 + \frac{\pi}{4}\int_{9/4}^{\infty}\lambda^3(\lambda-2)\frac{\tanh[\pi a(\lambda)]}{\cosh[\pi a(\lambda)]}\,d\lambda\right\}\Delta t^2 + O(\Delta t^3) \geqslant 0. \tag{92}$$

When we evaluate Eq. (92) with Eq. (87) in addition to Eq. (120),

$$\int_{9/4}^{\infty}\lambda^3(\lambda-2)\frac{\tanh[\pi a(\lambda)]}{\cosh[\pi a(\lambda)]}\,d\lambda = \frac{136}{\pi}, \tag{93}$$

and ignore the $O(\Delta t^3)$ term, we have

$$C_v - 12\Delta t - 36\Delta t^2 \geqslant 0. \tag{94}$$

Solving this quadratic equation for Δt and once more casting the resulting expression into dimensional units using Eqs. (26) and (29) gives

$$\Delta t \leqslant \frac{1}{6}\frac{1}{\sigma_{\mathrm{Th}} c}\frac{mc^2}{kT}\left[\sqrt{1+\frac{C_v(T)}{kN_p}}-1\right]. \tag{95}$$

To calculate either the exact time-step limits from Eqs. (78) and (91), along with Eqs. (26) and (29), or their approximate counterparts by employing Eqs. (89) and (95), or to determine whether a simulation is unconditionally stable through Eq. (85), we also need a value for the equilibrium material temperature. For our simplified radiative-transfer problem, combining conservation of energy and Eqs. (9) and (11) yields

$$U(T)+3kTN_p = U[T(0)]+\frac{1}{c}\iint I(v,\mathbf{\Omega},0)d\mathbf{\Omega}\,dv. \tag{96}$$

Here, $T(0)$ and $I(v,\mathbf{\Omega},0)$ are the initial material temperature and radiation intensity, respectively. Eqs. (3) and (96) form an expression for the equilibrium material temperature. Of course, for more complex radiative-transfer problems, Eq. (96) may need to be modified in order to account for a nonconstant photon density or a varying amount of total energy.

5. Numerical results

We now establish the effectiveness of our time-step limits using three test problems described by Eqs. (1) and (2). In these problems, the (temperature-independent) heat capacity is $C_v = 0.1$ GJ/keV/cm^3, the photon density is $N_p = 6.24\times10^{23}$ cm^{-3}, and the electron density is such that the Thomson opacity is $\sigma_{\mathrm{Th}} = 1$ cm^{-1}. For these problem parameters, Eqs. (12) and (85) indicate that it is possible to produce unstable solutions if the time-step size is sufficiently large.

To simulate these problems via Monte Carlo, we represent the total scattering opacity with a multigroup frequency structure and a frequency and temperature-dependent fit evaluated at group centers [18]. In addition, although we report the exact time-step limits for reference, we base our time-step sizes on the approximate time-step limits because they are much easier to calculate and, as we will see, fairly accurate. All simulations used 100,000 particles.

In the first problem we examine, the initial material temperature is 1.5 keV and the initial radiation intensity is isotropic and corresponds to a Wien distribution at 1 keV. For these initial conditions, the equilibrium material temperature is 1.125 keV, and the resulting approximate time-step limits are $\Delta t \leqslant 2.53$ ns to avoid instabilities and $\Delta t \leqslant 1.05$ ns to prevent nonphysical oscillations. As a comparison, the exact stability time-step limit is $\Delta t \leqslant 2.82$ ns and the exact oscillatory time-step limit is $\Delta t \leqslant 1.01$ ns. We simulated this problem with 1000 frequency groups uniformly spaced between 0 keV and 200 keV and time-step sizes of $\Delta t = 1.05$ ns (the approximate oscillatory time-step limit), 2.10 ns (twice the approximate oscillatory time-step limit), 2.53 ns (the approximate stability time-step limit), and 5.06 ns (twice the approximate stability time-step limit). The material temperature generated by these calculations is plotted in Figs. 2 and 3. From Fig. 2, we see that the material temperature monotonically decreases for $\Delta t = 1.05$ ns and nonphysically oscillates before reaching equilibrium for $\Delta t = 2.10$ ns. Also, Fig. 3 shows that the material temperature again nonphysically oscillates as it moves towards equilibrium for $\Delta t = 2.53$ ns, while further increasing the time-step size to $\Delta t = 5.06$ ns results in an unstable solution that even-

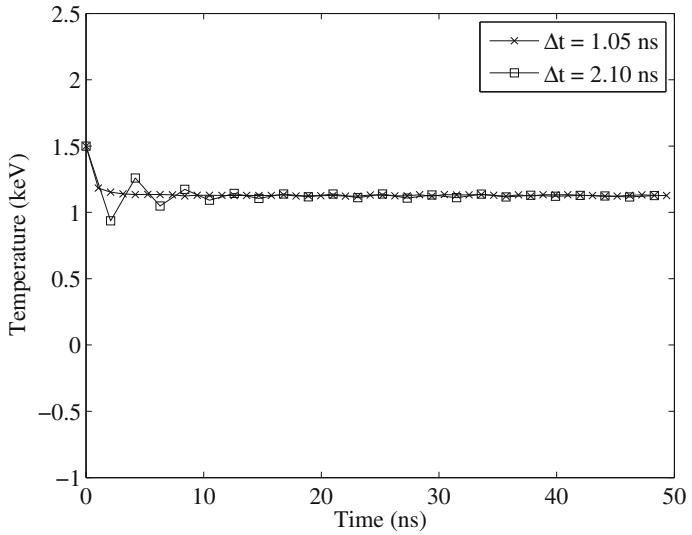

Fig. 2. First problem material temperature for Δt = 1.05 ns and 2.10 ns.

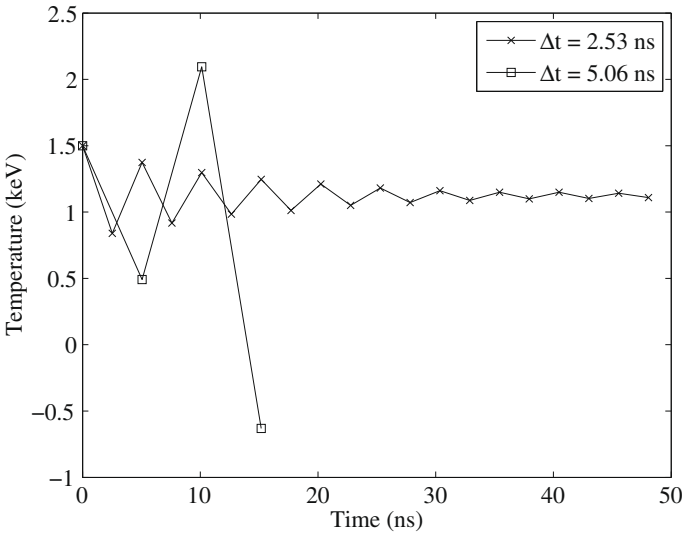

Fig. 3. First problem material temperature for Δt = 2.53 ns and 5.06 ns.

tually produces a negative material temperature. Of course, this negative material temperature causes the simulation to stop. We conclude that our time-step limits performed as intended for this problem; using the maximum time-step size avoids undesirable behavior (i.e., instabilities for the stability time-step limit and both instabilities and nonphysical oscillations for the oscillatory time-step limit), while doubling the time-step size yields undesirable behavior and demonstrates that our time-step limits are not overly conservative.

The second problem we consider is nearly identical to the first except the initial material temperature is 100 keV and thus the initial conditions are farther from equilibrium in this case. With these initial conditions, the equilibrium material temperature is 25.75 keV, and the corresponding approximate time-step limits are $\Delta t \leqslant 0.110$ ns to prevent instabilities and $\Delta t \leqslant 0.0457$ ns to avoid nonphysical oscillations. For reference, the exact stability time-step limit is $\Delta t \leqslant 0.123$ ns and the exact oscillatory time-step limit is $\Delta t \leqslant 0.0440$ ns. We simulated this problem using 200 frequency groups logarithmically spaced between 0.02 keV and 2000 keV and time-step sizes of $\Delta t = 0.0457$ ns (the approximate oscillatory time-step limit), 0.0914 ns (twice the approximate oscillatory time-step limit), 0.110 ns (the approximate stability time-step limit), 0.183 ns (four times the approximate oscillatory time-step limit), 0.220 ns (twice the approximate stability time-step limit), and 0.440 ns (four times the approximate stability time-step limit). The material temperature calculated by these simulations

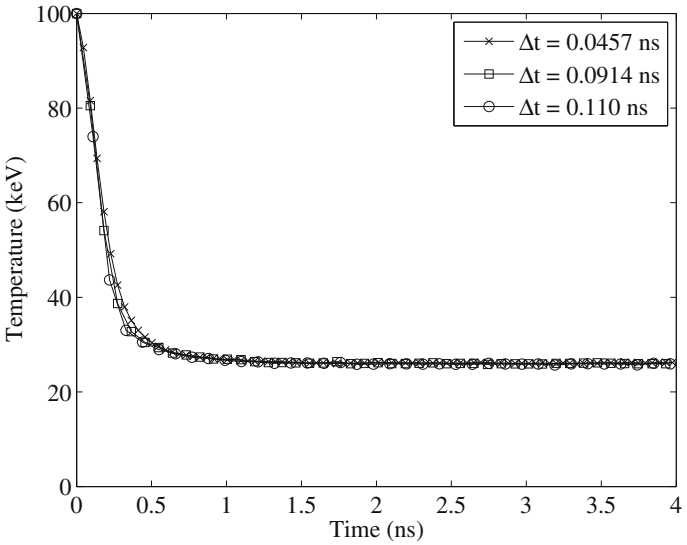

Fig. 4. Second problem material temperature for Δt = 0.0457 ns, 0.0914 ns, and 0.110 ns.

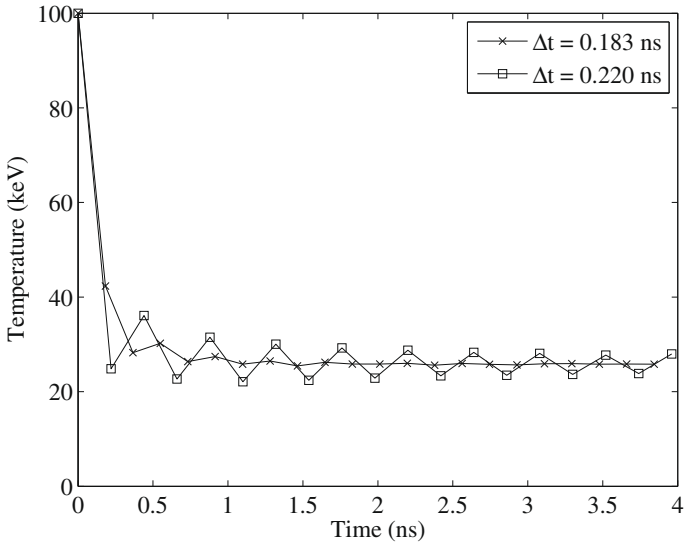

Fig. 5. Second problem material temperature for Δt = 0.183 ns and 0.220 ns.

is displayed in Figs. 4 and 5. We see from Fig. 4 that the material temperature monotonically approaches equilibrium for time-step sizes as large as $\Delta t = 0.110$ ns. In addition, Fig. 5 shows that the material temperature nonphysically oscillates but eventually reaches equilibrium for $\Delta t = 0.183$ ns and is barely stable for $\Delta t = 0.220$ ns. Employing a time-step size of $\Delta t = 0.440$ ns produced a negative material temperature at the end of the first time step instead of an unstable solution, and thus we do not present these results. Again, our time-step limits worked as designed, although they are conservative by at most factor of four in this problem as opposed to the factor of two in the previous problem.

The final problem we examine has an initial material temperature of 1 keV and an initial radiation intensity that is isotropic but represented by a delta function in frequency such that all photons begin with a frequency of $h\nu = 97.4$ keV (the center of group 148). These initial conditions yield an equilibrium material temperature of 24.6 keV, and the resulting approximate time-step limits are $\Delta t \leqslant 0.115$ ns to prevent instabilities and $\Delta t \leqslant 0.0478$ ns to avoid nonphysical oscillations. For comparison, the exact stability time-step limit is $\Delta t \leqslant 0.129$ ns and the exact oscillatory time-step limit is $\Delta t \leqslant 0.0460$ ns. We simulated this problem using the same frequency-group structure as in the previous problem and time-step sizes of $\Delta t = 0.0478$ ns (the approximate oscillatory time-step limit), 0.0956 ns (twice the approximate oscillatory

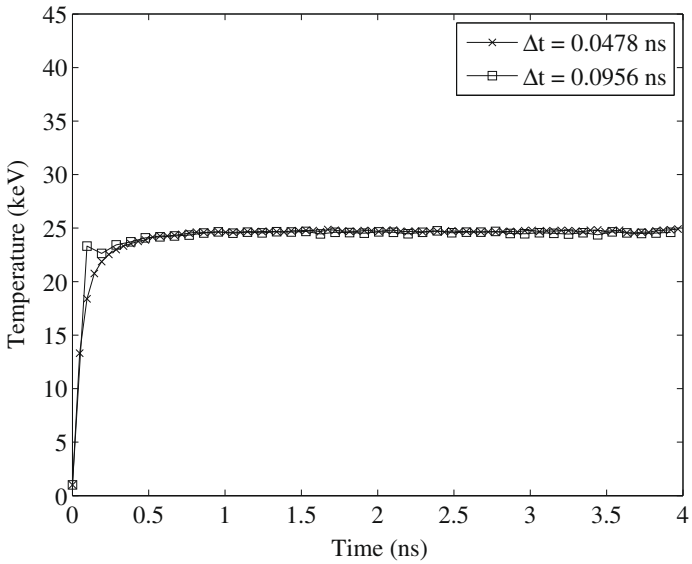

Fig. 6. Third problem material temperature for Δt = 0.0478 ns and 0.0956 ns.

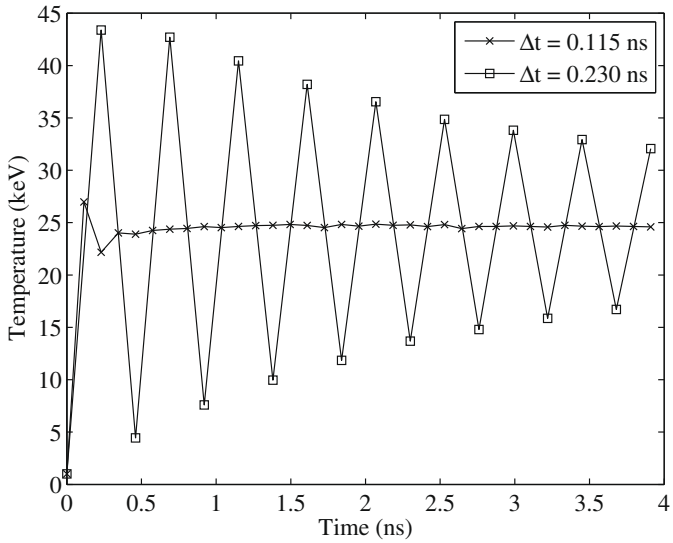

Fig. 7. Third problem material temperature for Δt = 0.115 ns and 0.230 ns.

time-step limit), 0.115 ns (the approximate stability time-step limit), 0.230 ns (twice the approximate stability time-step limit), and 0.460 ns (four times the approximate stability time-step limit). The material temperature produced by these calculations is plotted in Figs. 6 and 7. From Fig. 6, we see that the material temperature increases towards equilibrium without oscillating for $\Delta t = 0.0478$ ns and is nonmonotonic during the second time step for $\Delta t = 0.0956$ ns. Also, Fig. 7 shows that the material temperature is slightly more oscillatory for $\Delta t = 0.115$ ns than for $\Delta t = 0.0956$ ns and exhibits large nonphysical oscillations for $\Delta t = 0.230$ ns. We do not plot the material temperature for $\Delta t = 0.460$ ns as it is negative at the end of the second time step in lieu of being unstable. Thus, for this problem, our time-step limits are once more conservative by at most a factor of four, and we again conclude that they performed as intended.

6. Conclusions

We have performed a stability analysis of a Monte Carlo method for simulating Compton scattering in high energy density applications. With the results of this analysis, we have developed two time-step limits that avoid undesirable behavior. The first time-step limit prevents instabilities, while the second, more restrictive time-step limit avoids both instabilities and nonphysical oscillations. In fact, we have presented two versions of each time-step limit. The first version must be determined by solving a nonlinear inequality, whereas the second version is an approximation of the first that can be written in closed form. We have exclusively considered these approximate time-step limits because they are much easier to calculate and fairly accurate as compared to their exact counterparts.

We have demonstrated the efficacy of our time-step limits using a set of numerical examples. In these calculations, our time-step limits always performed as designed. Specifically, no undesirable behavior — instabilities for the stability time step limit and both instabilities and nonphysical oscillations for the oscillatory time-step limit — was observed when employing the maximum time-step size, whereas multiplying the time-step size by at most a factor of four generated undesirable behavior, which demonstrates that our time-step limits are not overly conservative. In future work, we plan on applying our time-step limits to more complex radiative-transfer problems that include the effects of absorption, emission, sources, and photon streaming.

Acknowledgments

This work was performed under US government contract DE-AC52-06NA25396 for Los Alamos National Laboratory, which is operated by Los Alamos National Security, LLC, for the US Department of Energy.

Appendix A. A proof that the amplification factors are real

To prove that there are no complex amplification factors, we assume that a complex amplification factor does exist, then show that this assumption leads to a contradiction. For a complex value of ω, we again avoid the singularities when solving Eqs. (63)–(65) and Eqs. (69)–(72) still hold,

$$\alpha_0 = 0, \tag{97}$$

$$\alpha_2 = \frac{1}{\sqrt{2}} \frac{1 - e^{-2\Delta t}}{\omega - e^{-2\Delta t}} \delta T, \tag{98}$$

$$\alpha_\lambda = \frac{\beta_\lambda}{\lambda} \frac{1 - e^{-\lambda \Delta t}}{\omega - e^{-\lambda \Delta t}} \delta T, \tag{99}$$

and

$$C_v \delta T + 3\sqrt{2}\alpha_0 + \sqrt{2}\alpha_2 + \int_{9/4}^{\infty} \frac{2}{\lambda} \beta_\lambda \alpha_\lambda = 0. \tag{100}$$

Multiplying Eqs. (98)–(100) by the complex conjugate of δT yields

$$\delta T^* \alpha_2 = \frac{1}{\sqrt{2}} \frac{1 - e^{-2\Delta t}}{\omega - e^{-2\Delta t}} |\delta T|^2, \tag{101}$$

$$\delta T^* \alpha_\lambda = \frac{\beta_\lambda}{\lambda} \frac{1 - e^{-\lambda \Delta t}}{\omega - e^{-\lambda \Delta t}} |\delta T|^2, \tag{102}$$

and

$$C_v |\delta T|^2 + 3\sqrt{2}\delta T^* \alpha_0 + \sqrt{2}\delta T^* \alpha_2 + \int_{9/4}^{\infty} \frac{2}{\lambda} \beta_\lambda \delta T^* \alpha_\lambda \, d\lambda = 0. \tag{103}$$

The complex conjugates of Eqs. (101)–(103) are

$$\delta T \alpha_2^* = \frac{1}{\sqrt{2}} \frac{1 - e^{-2\Delta t}}{\omega^* - e^{-2\Delta t}} |\delta T|^2, \tag{104}$$

$$\delta T \alpha_\lambda^* = \frac{\beta_\lambda}{\lambda} \frac{1 - e^{-\lambda \Delta t}}{\omega^* - e^{-\lambda \Delta t}} |\delta T|^2, \tag{105}$$

and

$$C_v |\delta T|^2 + 3\sqrt{2}\delta T \alpha_0^* + \sqrt{2}\delta T \alpha_2^* + \int_{9/4}^{\infty} \frac{2}{\lambda} \beta_\lambda \delta T \alpha_\lambda^* \, d\lambda = 0, \tag{106}$$

where we have employed the fact that C_v, Δt, λ, and β_λ are real [see Eq. (48)]. When we subtract Eq. (106) from (103), we have

$$3\sqrt{2}(\delta T^* \alpha_0 - \delta T \alpha_0^*) + \sqrt{2}(\delta T^* \alpha_2 - \delta T \alpha_2^*) + \int_{9/4}^{\infty} \frac{2}{\lambda} \beta_\lambda (\delta T^* \alpha_\lambda - \delta T \alpha_\lambda^*) d\lambda = 0. \tag{107}$$

Evaluating this expression with Eqs. (97), (101), (102), (104), and (105) gives

$$(\omega^* - \omega)|\delta T^2| \left[\frac{1 - e^{-2\Delta t}}{|\omega - e^{-2\Delta t}|^2} + 2 \int_{9/4}^{\infty} \left(\frac{\beta_\lambda}{\lambda} \right)^2 \frac{1 - e^{-\lambda \Delta t}}{|\omega - e^{-\lambda \Delta t}|^2} \, d\lambda \right] = 0. \tag{108}$$

Except for the trivial solution where $\delta T = 0$, Eq. (108) is only satisfied if $\omega = \omega^*$, which implies that the amplification factor is real. However, this statement contradicts our assumption, and we conclude that there are no complex amplification factors.

Appendix B. Evaluation of Eqs. (81), (87), and (93)

In this appendix, we demonstrate how to evaluate integrals of the form

$$\int_{9/4}^{\infty} \lambda^m (\lambda - 2) \frac{\tanh[\pi a(\lambda)]}{\cosh[\pi a(\lambda)]} d\lambda, \tag{109}$$

where m = 1, 2, and 3. First, we define a change of variables through Eq. (38),

$$\lambda = a^2 + \frac{9}{4}. \tag{110}$$

This expression allows us to write Eq. (109) as

$$\int_{9/4}^{\infty} \lambda^m (\lambda - 2) \frac{\tanh[\pi a(\lambda)]}{\cosh[\pi a(\lambda)]} d\lambda = \int_0^{\infty} 2a \left(a^2 + \frac{9}{4} \right)^m \left(a^2 + \frac{1}{4} \right) \frac{\tanh(\pi a)}{\cosh(\pi a)} da. \tag{111}$$

We can then calculate the right side of Eq. (111) using [19]

$$\int_0^\infty a^{2k+1}\frac{\tanh(\pi a)}{\cosh(\pi a)}\,da = \frac{2k+1}{\pi}\left(\frac{1}{2}\right)^{2k+1}|E_{2k}|, \quad k = 0, 1, \ldots \tag{112}$$

Here, E_{2k} is an Euler number, examples of which are [19]

$$E_0 = 1, \tag{113}$$
$$E_2 = -1, \tag{114}$$
$$E_4 = 5, \tag{115}$$
$$E_6 = -61, \tag{116}$$

and

$$E_8 = 1385. \tag{117}$$

A straightforward combination of Eqs. (111)–(117) yields

$$\int_{9/4}^\infty \lambda(\lambda-2)\frac{\tanh[\pi a(\lambda)]}{\cosh[\pi a(\lambda)]}\,d\lambda = \frac{4}{\pi}, \tag{118}$$
$$\int_{9/4}^\infty \lambda^2(\lambda-2)\frac{\tanh[\pi a(\lambda)]}{\cosh[\pi a(\lambda)]}\,d\lambda = \frac{20}{\pi}, \tag{119}$$

and

$$\int_{9/4}^\infty \lambda^3(\lambda-2)\frac{\tanh[\pi a(\lambda)]}{\cosh[\pi a(\lambda)]}\,d\lambda = \frac{136}{\pi}. \tag{120}$$

References

[1] G.C. Pomraning, The Equations of Radiation Hydrodynamics, Pergamon Press, Oxford, United Kingdom, 1973.
[2] E. Canfield, W.M. Howard, E.P. Liang, Inverse Comptonization by one-dimensional relativistic electrons, Astrophys. J. 323 (1987) 565.
[3] J.D. Densmore, J.S. Warsa, R.B. Lowrie, Time-step limits for a Monte Carlo Compton-scattering method, in: Proceedings of the International Conference on Mathematics, Computational Methods and Reactor Physics, Saratoga Springs, New York, 2009.
[4] J.A. Fleck Jr., J.D. Cummings, An implicit Monte Carlo scheme for calculating time and frequency dependent nonlinear radiation transport, J. Comput. Phys. 8 (1971) 313.
[5] T. N'kaoua, Solution of the nonlinear radiative transfer equations by a fully implicit matrix Monte Carlo method coupled with the Rosseland diffusion equation via domain decomposition, SIAM J. Sci. Stat. Comput. 12 (1991) 505.
[6] A.S. Kompaneets, The establishment of thermal equilibrium between quanta and electrons, Sov. Phys. JETP 4 (1957) 730.
[7] J.I. Katz, High Energy Astrophysics, Addison-Wesley Publishing, Menlo Park, CA, 1987.
[8] G.B. Rybicki, A.P. Lightman, Radiative Processes in Astrophysics, Wiley-VCH, Weinheim, Germany, 2004.
[9] J.I. Castor, Radiation Hydrodynamics, Cambridge University Press, Cambridge, United Kingdom, 2004.
[10] J.D. Densmore, J.S. Warsa, R.B. Lowrie, J.E. Morel, Stability analysis of implicit time discretizations for the Compton-scattering Fokker–Planck equation, J. Comput. Phys. 228 (2009) 5933.
[11] M. Abramowitz, I.A. Stegun, Handbook of Mathematical Functions with Formulas, Graphs, and Mathematical Tables, Dover Publications, Mineola, New York, 1970.
[12] D. Mihalas, B. Weibel-Mihalas, Foundations of Radiation Hydrodynamics, Dover Publications, Mineola, New York, 1999.
[13] H. Kahn, Applications of Monte Carlo, AECU–3259, Rand Corporation, 1954.
[14] R.N. Blomquist, E.M. Gelbard, An assessment of existing Klein–Nishina Monte Carlo sampling methods, Nucl. Sci. Eng. 83 (1983) 380.
[15] G.C. Pomraning, An eigenfunction description of radiative transfer in scattering atmospheres, Astrophys. J. 152 (1968) 809.
[16] A. Erdélyi, Higher Transcendental Functions, vol. 1, McGraw-Hill Book Company, New York, New York, 1953.
[17] J.C. Strikwerda, Finite Difference Schemes and Partial Differential Equations, Society for Industrial and Applied Mathematics, Philadelphia, PA, 2004.
[18] B.R. Wienke, Relativistic photon-Maxwellian electron cross sections, Astron. Astrophys. 152 (1985) 336.
[19] I.S. Gradshteyn, I.M. Ryzhik, Table of Integrals, Series, and Products, Academic Press, San Diego, CA, 2000.